Metals & corrosion

Investigation on crack behavior of Ni60A alloy coating produced by coaxial laser cladding

Bowen Shi[1,*] ![ORCID], Tao Li[1], Dong Wang[1], Xiaorui Zhang, and Hongchao Zhang[2]

[1] *School of Mechanical Engineering, Dalian University of Technology, Dalian 116024, China*
[2] *Department of Industrial, Manufacturing and Systems Engineering, Texas Tech University, Lubbock 79409, USA*

ABSTRACT

Crack is one of the common problems in preparation of NiCrBSi alloy coatings by laser cladding, especially for high hardness coatings. In this study, the crack behavior and prevention of Ni60A coating by coaxial laser cladding are investigated. The results indicate that the nonuniform hard Cr-rich precipitates and large residual tensile stress are the main reason for cracking of Ni60A coating. According to the difference of thermophysical properties and temperature between the coating and the substrate, the thermal stress models are established, in which the stress perpendicular to the scanning direction σ_y is smaller than the stress along the scanning direction σ_x. Due to the change in the relative relationship among σ_x, σ_y and fracture strength σ_f, the crack distribution changes from network to parallel, until to no crack with the increasing line energy and the decreasing powder feed rate. And the angle θ_0 between the direction of resultant stress of σ_x and σ_y and Y-axis is 52.85°, which fits with the direction of long and short cracks in network crack distribution. In addition, the substrate preheating can effectively reduce cracking rate of Ni60A coating and completely prevent crack when preheated up to 500 °C. Also, the crack-free coating can be obtained by the combination of preheating to 300 °C and placing insulated plank under the substrate, which can reduce thermal damage of the substrate and obtain higher microhardness.

Ⓐ Springer

Introduction

Laser cladding is a surface process producing high quality coating with a high power laser beam. Compared with other conventional surface techniques including the induction cladding, TIG welding and thermal spraying, laser cladding has some significant advantages such as low dilution, small heat-affected zone (HAZ), little deformation, high depositing efficiency and metallurgical bonding with substrate. Thus, it can be utilized in reconditioning worn components, deposition coatings with special properties, and manufacturing special structural parts [1–3]. The coaxial laser cladding, feeding powder coaxially to the laser beam, is easy to realize automation and large-area cladding. Its schematic diagram is described in Fig. 1. However, crack occurs in the cladding layer frequently due to the large thermal stress and the interaction of many factors, such as complex microstructure, large amount of defects, mismatched thermophysical properties of cladding layer and substrate, et al., which is the biggest problem to promote the laser cladding technology [4–6]. Especially, it is difficult to obtain high hardness crack-free coating on steel substrate by coaxial laser cladding without assistive technology [7, 8].

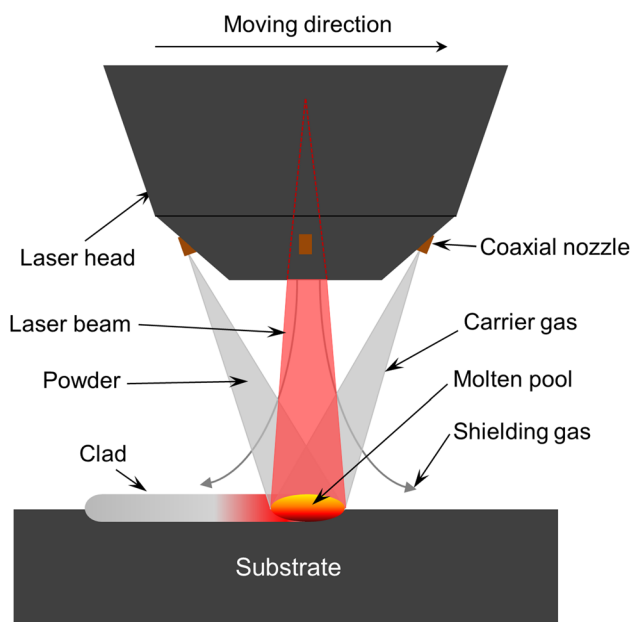NiCrBSi alloys have been widely used in laser cladding owing to the outstanding wear, corrosion,

oxidation resistance and relatively low cost. Ni60A is one of NiCrBSi alloys with high hardness up to 58–62 HRC. Due to the rapid heating and cooling cycle in laser cladding, large amount of less-favorable microstructures such as hard Cr-rich precipitates and Ni–B–Si eutectic structures are produced, which shows high hardness, wear resistance but a high cracking susceptibility [4, 9]. Generally, crack occurs when the residual stress exceeds the yield strength or the local plasticity is insufficient to accommodate the induced plastic deformation, which often happens in laser cladding of NiCrBSi alloys [10]. According to the simulation results of cladding Ni60 powder on type 1045 steel plate [11], the tensile stress along scanning direction was up to 2 cxGPa, which was much larger than the stress vertical scanning direction. And the tensile plastic strain along scanning direction is greatest at the peak of the track. As a result, the transverse crack can be easily initiated at the peak of the track, which is decided by the solidification characteristics and microstructure. Huang et al. [8, 12] researched that there was another peak value of tensile stress in the bottom of the coating owing to martensitic transformation in HAZ. It also can lead to crack initiation. Then, the crack propagated along the nonuniformly distributed hard precipitates and eutectic structures under residual tensile stress [13]. Eventually, the crack ran through entire surface of the coating, forming various crack distributions on the coating surface. The crack is detrimental to the mechanical properties of the coating, leading to failure of cladding.

In order to prevent cracking of Ni60A coating, the residual stress must be reduced and the coarse hard precipitates must be refined. Many methods have been proposed to reduce cracking sensitivity of Ni60A coating, such as optimizing process parameters [14], preheating the substrate [8], controlling content of alloy elements [15–17], introducing electromagnetic field [18] or ultrasonic vibration [19]. Wang et al. [20] studied the crack of Ni60A coating online by acoustic emission technique, and the results shown that the main form of cracks was cold crack and its initiation and propagation mainly concentrated from 600 °C to 400 °C in cooling. Generally, preheating the substrate prior to laser cladding is an effective method to reduce cracking susceptibility by decreasing the temperature gradient between the coating and substrate. Jendrzejewski et al. [21, 22] studied that the residual stress of the coating

Figure 1 Schematic diagram of coaxial laser cladding process.

decreases from 1800 to 900 MPa when preheated to 500 °C, which can obtain crack-free coating. While, the high preheating temperature will cause thermal damage and mechanical property worsening of the substrate, especially for the carbon steel substrate [23].

In previous studies, little notice has been paid on the relationship between crack distribution and the relative change in thermal stress caused by different process parameters, and this aspect is helpful to research the crack behavior and prevention. In this study, Ni60A alloy coating is prepared on 45 steel substrate by coaxial laser cladding, and the crack behavior of cladding layer is studied based on the different process parameters. The thermal tress model is established to study the influence of process parameters on crack distribution, including the relationship between crack direction and thermal stress direction. In addition, in order to prevent crack of Ni60A coating with a relatively low preheating temperature, an insulated plank is placed under the substrate to reduce the cooling rate further. This study provides a reference for preparing crack-free Ni60A alloy coating by coaxial laser cladding.

Experiment procedures

The coaxial laser cladding system consists of five subsystems, LDF 4000-100 4 kW YAG laser, Raycham RC-PF-01B-2 mental powder feeder, KUKA KE30HA six-axes robot, Precitec YC52 laser cladding head with four coaxial nozzles, MCWL-150T-01AK1S4 precision chiller with recirculated water. The cladding material is Ni60A alloy powder with the size of 36–150 μm and spherical shape. The substrate is 45 steel plate which is a kind of high-quality carbon structural steel, and its size is 40 mm × 30 mm × 8 mm. The chemical composition of this cladding material and substrate is listed in Table 1. Before laser cladding, the powder is placed in a drying chamber at 120 °C for 2 h to remove moisture in powder, and

the substrate surface is ground with an angle grinder and cleaned with acetone. Argon with 99.99% purity is used as the carrier gas and shielding gas with flow rate of 400 L/h. The multi-track cladding tests have 10 tracks with 40% overlapping ratio. The parameters used in this study are shown in Table 2.

After laser cladding, the surface cracks of the Ni60A coating are characterized by dye penetration test. The cracking rate R is assessed via the crack number in unit cladding length [8], i.e., the ratio of the total crack number to the total cladding length. The cross section of specimens is chemically etched with a mixed acid consisting of 75 vol.% HCl and 25 vol.% HNO$_3$. The microstructure is analyzed using the optical microscope (OM) and the scanning electronic microscope (SEM). The X-ray diffractometer (XRD) is utilized for phase identification. The microhardness is measured using a Vickers Tester with a load of 3 N and a dwelling time of 15 s. Two-color pyrometer with 60 Hz sampling frequency is applied to measure molten pool temperature utilizing paraxial measurement method. Thermocouple with 100 Hz sampling frequency is welded on the substrate surface to measure substrate temperature.

Analysis and results

Crack morphology

The cracking behavior can be described by the cracking rate and crack morphology. The macroscopic crack distribution of Ni60A coating using dye penetrant test is shown in Fig. 2. The random distributed annular cracks are approximately perpendicular to the scanning direction in single-track cladding. While, there is network crack distribution in multi-track cladding that consists of some long cracks and more short cracks.

According to the stress intensity factor theory of crack propagation [24], the critical stress intensity factor of crack propagation decreases with the increasing crack length, and the next track has similar

Table 1 Chemical composition (wt%) of Ni60A alloy powder and 45 steel plate

	C	B	Cr	Si	Mn	Cu	P, S	Fe	Ni
Ni60A	0.8–1.0	3.1–3.8	15.5–17.8	3.8–4.5	–	–	–	3.5 ∼ 4.5	Bal
45 steel	0.42–0.5	–	≤ 0.25	0.17–0.37	0.5–0.8	≤ 0.25	≤ 0.045	Bal	≤ 0.25

Table 2 Process parameters of experiment

Parameters	Laser power (W)	Scanning speed (mm/s)	Powder feed rate (g/s)	Laser spot size (mm)
Value	800–2000	1.5–9	0.087–0.272	3
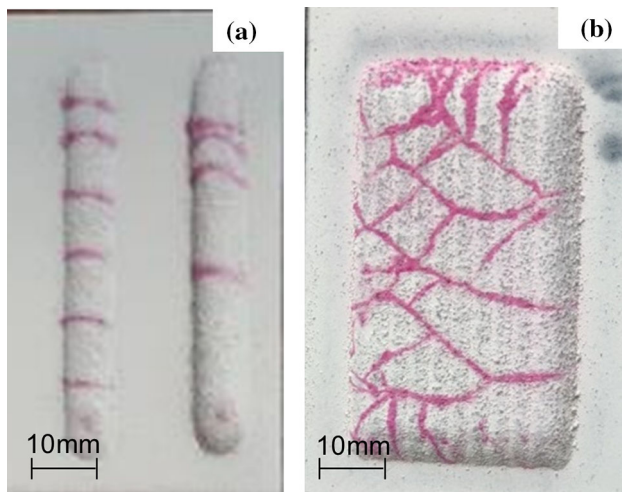
Figure 2 Macroscopic crack morphology of Ni60A coating.

lattice orientation with the previous track. Due to similar thermal stress of each track, the crack in the preceding track unstable propagates to next lapped track. Therefore, it is possible to study the cracking of multi-track cladding by studying the cracking of single-track cladding with the same process parameters.
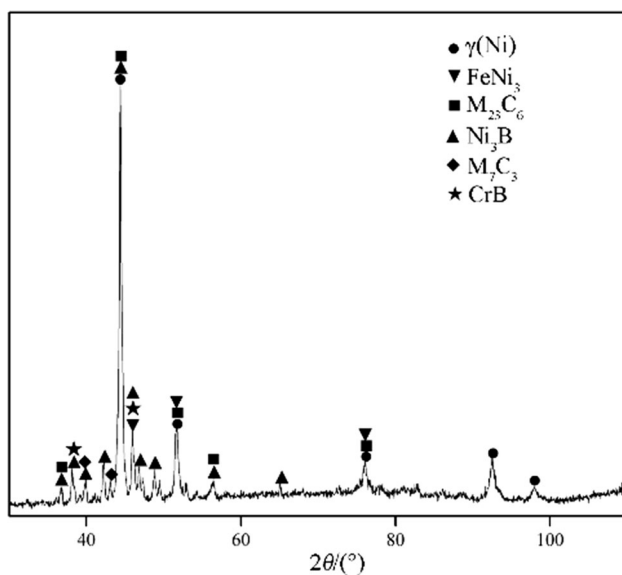
Figure 3 XRD patterns of Ni60A coating.

The XRD pattern of Ni60A coating is shown in Fig. 3. Combined with SEM analysis [14], the matrix phase of the coating is γ-Ni, and hard precipitates $M_{23}C_6$ (M=Cr, Ni, Fe), M_7C_3, CrB nonuniformly distribute in the coating. Also, there is a certain amount of eutectic and amorphous phases such as $FeNi_3$/Ni, Ni_3B, et al. According to the formation temperature of each phase [25], CrB is the first phase to form, and then Cr_7C_3 and $Cr_{23}C_6$ nucleate on precipitated CrB particles. As the temperature continues to drop, γ-Ni solid solution forms, and the eutectics and amorphous are the last formed phases. The presence of hard precipitates such as Cr_7C_3, $Cr_{23}C_6$, CrB can enhance the hardness of coating but leads to high brittleness.

Due to nonequilibrium solidification process, the hard precipitates form quickly and nonuniformly, which induces serious crystal lattice distortion and high level of internal stress inside the hard precipitates [10]. It leads to cracking of the hard precipitates eventually, liking the marked precipitates by the red line in Fig. 4a. Meanwhile, the crack propagation has obvious selectivity, which the crack deflects when encounters gray–white γ-Ni, and continues to propagate when encounters gray–black blocky CrB or dendritic Cr_7C_3 [14] until the end of the crack. These large amounts and nonuniformly distributed Cr-rich precipitates provide easy routes for crack propagation. Due to the defects in production of Ni60A particle, there are serious microcracks in the large incomplete melting powder at the top of coating after cladding, as shown in Fig. 4b. These microcracks in hard precipitate and incomplete melting powder result in crack initiation and propagation under the residual tensile stress. Therefore, there is high cracking susceptibility of Ni60A coating prepared by coaxial laser cladding.

The influence of process parameters on cracking rate

In order to simplify the process parameters which have the greatest influence on cracking rate, the
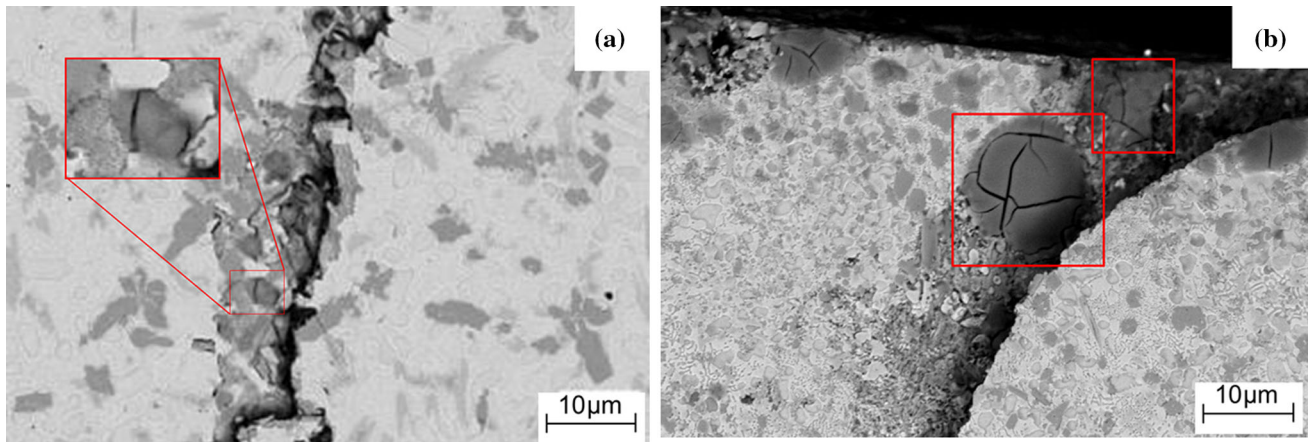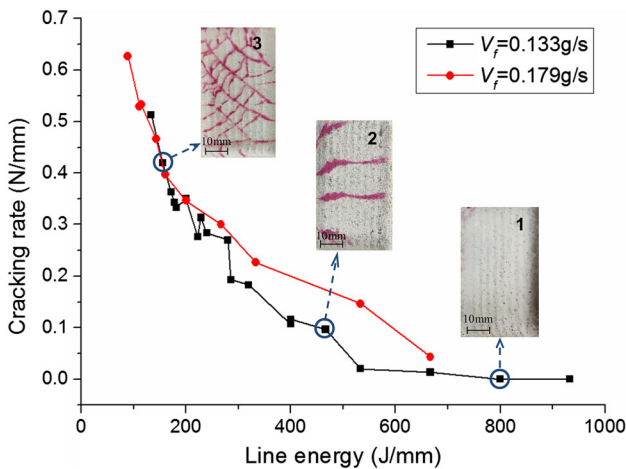
Figure 4 SEM backscatter crack image.

Figure 5 Influence of line energy on cracking rate.

Figure 6 Influence of powder feed rate on cracking rate.

indirect process parameter, line energy, is selected. The line energy is the ratio of power to scanning speed. As shown in Fig. 5, the cracking rate decreases obviously with the increasing line energy at the same powder feed rate. When the line energy is high, the molten pool can obtain more energy to melt powder particles completely, and the dwell time of molten pool increases to reduce the cooling rate and defects in coating. The lower cooling rate benefits high-temperature plastic flow and stress relaxation of the coating [12, 26], and the few defects can improve the fracture strength. Also, the larger dilution rate increases plasticity of Ni60A coating and reduces cracking due to the more energy obtained by substrate [27]. In Fig. 5, the crack-free Ni60A coating can be obtained when the line energy is up to 800 J/mm in the condition $V_f = 0.133$ g/s. Therefore, large line
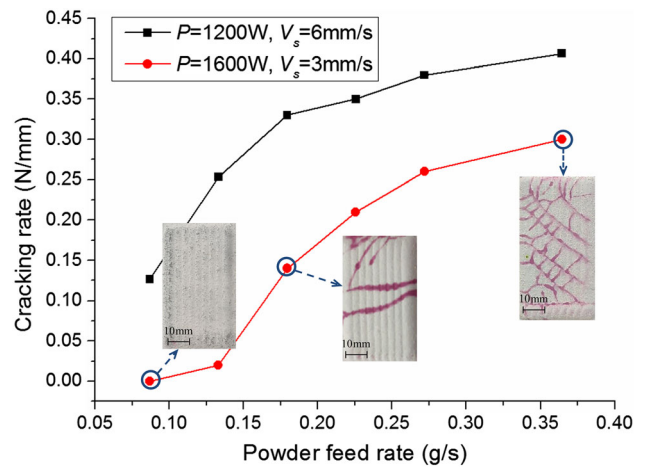
energy is helpful to prevent crack when the line energy suitably matches the powder feed rate.

The powder feed rate has a great influence on cracking by control the amount of powder injected into the molten pool. As shown in Fig. 6, the crack firstly increases sharply and then slowly with the increasing powder feed rate. When the powder feed rate is large, the obtained energy of unit mass powder is small. As a result, the small energy can increase cooling rate, leading to high residual stress in coating. Also, due to lack of sufficient energy, there are severe structure inhomogeneity and large hard precipitates in the coating, which increases defects and reduces fracture strength. Meanwhile, the shading rate of powder to laser increases with the increasing powder feed rate, leading to low dilution rate and plasticity of coating, which contributes to cracking. In Fig. 6, the crack-free Ni60A coating can be obtained when the

powder feed rate is down to 0.087 g/s in the condition $P = 1600$ W and $V_s = 3$ mm/s. Therefore, lower powder feed rate is selected possible to prevent crack on the premise of performance and size requirement.

The influence of substrate preheating on cracking rate

Although the crack can be avoided by optimizing process parameters, the available parameter range is too small and the dilution rate is large to reduce the hardness of Ni60A coating drastically. While the substrate preheating is an appropriate method to obtain no-crack coating with high performance. In this paper, the preheating process is air cooling after cladding.

The preheating laser cladding (pre-LC) can reduce temperature gradient between the coating and the substrate effectively. The quantitative relationship between temperature gradient and preheating temperature is [6]

$$G_{cs} = \frac{2\pi\lambda_c \left(T_{liq} - T_{pre}\right)^2}{\beta_c P} \tag{1}$$

where G_{cs} is the temperature gradient between coating and substrate, T_{liq} is the liquidus temperature of Ni-based self-fluxing alloy, T_{pre} is the preheating temperature of the substrate, β_c is laser absorptivity of the coating, λ_c is thermal conductivity of the coating. In Eq. (1), the temperature gradient decreases rapidly with the increasing preheating temperature. The thermal stress is positively correlated with the temperature gradient [4], so the substrate
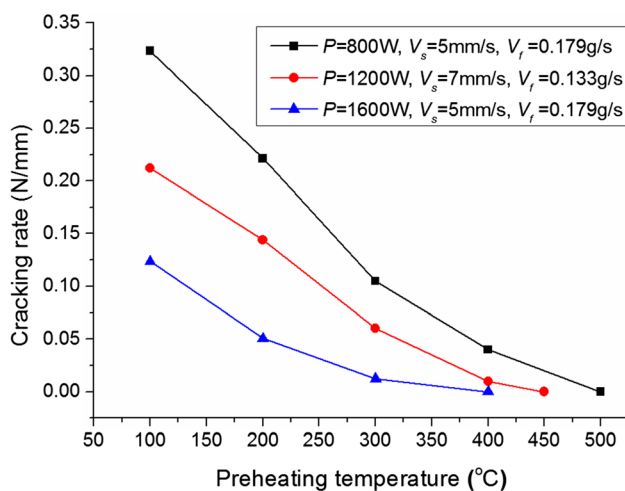
preheating plays a significant role in reducing thermal stress and cracking susceptibility.

The cracking rate decreases with the increasing preheating temperature as shown in Fig. 7, and crack is completely prevented for most process parameters when the preheating temperature is up to 500 °C. The substrate preheating can reduce cooling rate partly, which can not only prolong the dwell time of high temperature to relax residual stress but also reduce the defects to improve the fracture strength of coating. So, it helps to obtain crack-free Ni60A coating. For the higher line energy and lower powder feed rate, the need preheating temperature to prevent crack is lower.

Discussions

Thermal stress model

Due to the great difference of thermophysical properties and temperature between Ni60A alloy coating and 45 steel substrate, the thermal stress is the main part of residual stress and has a crucial influence on cracking [28]. When the powders and the substrate surface are instantaneously melted by laser beam, the volume expansion occurs and the stress is compressive, and then the compressive stress can be quickly relaxed to near zero due to the fluidity of liquid. The cooling process can be divided into two stages. The first stage is cooling from peak temperature to the solidus curve, and the tensile stress caused by volume contraction also is relaxed to near zero due to the fluidity of liquid. The second stage is cooling from the solidus curve to room temperature, and the tensile stress at this stage is the main source of residual stress in the coating [6].

Because the coefficient of thermal expansion of coating is larger than that of substrate, the simplified residual stress model for LC is established based on the elastic mechanics. The deformation of coating is $\alpha_c l\Delta T - l\sigma_x/E_c$, and according to previous research [29], the thermal stress in X direction σ_x is

$$\sigma_x = \frac{E_c E_s h_s (\alpha_c - \alpha_s)\Delta T}{(1 - \mu)(E_s h_s + E_c h_c)} \tag{2}$$

where μ is Poisson ratio of the coating, α, E, h are defined as coefficient of thermal expansion (CTE), elastic modulus and thickness, respectively, and the subscripts c and s represent the coating and the

Figure 7 Influence of preheating temperature on cracking rate.

substrate, respectively, ΔT is the difference between the actual crystallization temperature of the molten pool and the ambient temperature, l is the length of the clad track at initial state.

Taking the influence of Poisson ratio μ on deformation, the deformation in X direction is larger to effect the deformation in Y direction. Thus, the thermal stress in Y direction of single-track σ_{y1} is

$$\sigma_{y1} = \frac{E_c E_s h_s (\alpha_c - \alpha_s) \Delta T}{(E_s h_s + E_c h_c)} \tag{3}$$

Due to the deformation caused by the large thermal stress, a certain displacement relative to the substrate occurs. Correspondingly, a shear strain τ_{zx} on the substrate surface occurs to hinder the deformation.

Assume that the stress distributed uniformly in the coating. For any section dx of a single track as shown in Fig. 8, the following equation can be obtained obeying the internal force balance principle,

$$(\sigma_x + d\sigma_x)wh - \sigma_x wh - \tau_{zx} w dx = 0 \tag{4}$$

A bending moment occurs due to the exist of τ_{zx}, which will cause a warping deformation of the track. However, due to the stress in Z direction σ_z caused by the constraint of the substrate, there is no warping of the track. The bending moment caused by σ_z is balanced by the bending moment caused by the stress τ_{zx}, that is

$$\frac{h}{2} \int_0^x w \tau_{zx} dx = \int_0^x w \sigma_z x dx \tag{5}$$

According to Eqs. (4) and (5), the maximum of σ_z occurs at the edge of the track at $x = l$,
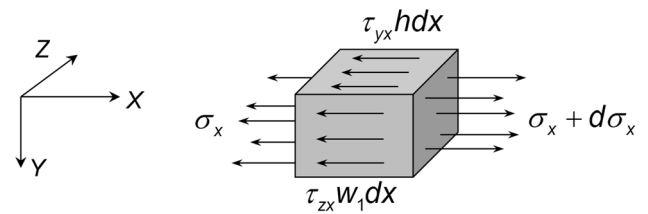
Figure 9 Stress analysis in X direction of the new deposited track.

$$\sigma_z = \frac{h^2}{l^2} \sigma_x \tag{6}$$

Thus, a limited toe crack can occur at the edge of track due to σ_z in the multi-layer cladding [11].

As shown in Fig. 9, for any section dx of a new deposited track in multi-track cladding, the following equation can be obtained obeying the internal force balance principle,

$$(\sigma_x + d\sigma_x)wh - \sigma_x w_1 h - \tau_{zx} w_1 dx - \tau_{yx} h dx = 0 \tag{7}$$

where the width of the new deposited track connected with the substrate is only 60% of the first track width due to 40% overlapping ratio, that is $w_1 = 0.6w$.

Due to the exist of τ_{yx}, a bending moment to the new deposited track occurs. And, due to the stress σ_{y2} caused by the constraint of previous track, the bending moment caused by σ_{y2} is balanced by the bending moment caused by the stress τ_{yx}, that is

$$\frac{w}{2} \int_0^x h \tau_{yx} dx = \int_0^x h \sigma_{y2} x dx \tag{8}$$

According to Eqs. (7) and (8),

Figure 8 Stress analysis in X direction of the single track.
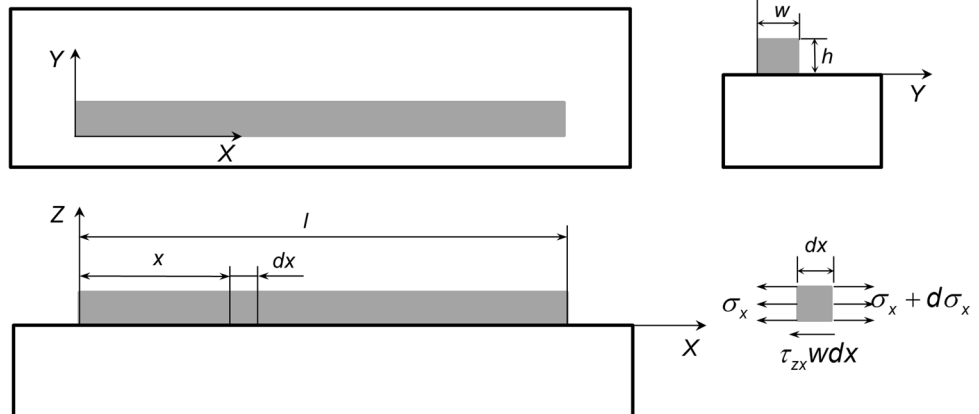
$$\sigma_{y2} = \frac{2}{5}\frac{w^2}{l^2}\sigma_x \tag{9}$$

It shows that σ_{y2} increases with the increasing cladded width w.

Thus, the thermal stress in Y direction of the multi-track cladding is

$$\sigma_y = \sigma_{y1} + \sigma_{y2} = \left(\frac{2}{5}\frac{w^2}{l^2(1-\mu)}+1\right)\frac{E_cE_sh_s(\alpha_c-\alpha_s)\Delta T}{(E_sh_s+E_ch_c)} \tag{10}$$

The relationship of thermal stress and crack distribution

The basic reason of Ni60A coating cracking is that the tensile stress in the coating exceeds the fracture strength σ_f. In above thermal stress models, the height h and the width w are much smaller than the length l, so the σ_z is much smaller than σ_{y1} and σ_x, and σ_{y1} is smaller than σ_x, which has been proven in some researches [11, 21]. As a result, there is generally annular cracks perpendicular to X direction on the track, as shown in Fig. 2a.

In the multi-track cladding, the crack distribution changes due to the change in the relative relationship among σ_x, σ_y and fracture strength σ_f. As shown in Fig. 5, there is no macrocrack on No. 1 coating due to high line energy. In this situation, low cooling rate reduces the residual stress significantly, and large dilution rate improves fracture strength dramatically. So $\sigma_x < \sigma_f$ to obtain no macrocrack coating. There are several large long cracks perpendicular to scanning direction on No. 2 coating due to medium line energy. In this situation, the medium cooling rate reduces the residual stress partly, and a certain dilution rate improves fracture strength partly. So $\sigma_y < \sigma_f < \sigma_x$ to form several almost parallel cracks under σ_x only. There are network cracks on No. 3 coating due to low line energy. In this situation, high cooling rate has almost no influence on the tensile stress reduction, and little dilution rate has almost no influence on fracture strength improvement. So $\sigma_y > \sigma_f$ to form network crack distribution under the resultant stress of σ_x and σ_y. In some cases, the network crack change to parallel crack as the track number increases. This is because σ_y reduces to below σ_f caused by the heat accumulation effect on the substrate, as shown in Fig. 2b. There are same crack distribution in the experiment results with the increasing powder feed rate. The study of crack distribution change caused by different process parameter is helpful to obtain crack-free Ni60A coatings.

As shown in Fig. 10a, the network crack distribution is composed of some long cracks incline to the scanning direction and some short cracks connected two adjacent long cracks. The angle θ between the long crack and the scanning direction is $50° \sim 54°$. And the angle between the direction of resultant stress of σ_x and σ_y and Y-axis $\theta_0 = \arctan(\sigma_x/\sigma_y) = 52.85° \in (50°, 54°)$, which fits with the observed results. Due to the heat accumulation effect on the substrate, the continuous long cracks incline to the scanning direction. Thus, the thermal stress models have certain credibility. Generally, the short crack is inclined to the opposite direction of scanning (i.e., minus X direction) and extends to the adjacent long crack crossing one or several tracks. As shown in Fig. 10b, σ_L and σ_S are the resultant stress causing long and short crack, respectively, and they are symmetric with Y-axis due to the symmetry of σ_x. As a result, the angle of short crack and minus X direction also is θ, and the X component of the extension direction of long and short crack can be canceled to achieve balance. There are stress mutation and relatively coarse structure at the overlap joint of two tracks [14] where the short crack intersects with the long crack.

As shown in Fig. 11, the crack distribution of the coating changes significantly with the increasing preheating temperature, which changes from network to parallel, until to no crack. Due to the smaller temperature gradient and lower cooling rate, the residual stress of Ni60A coating reduces gradually with the increasing preheating temperature. Because $\sigma_y < \sigma_x$, and firstly σ_y reduces to below σ_f with the crack distribution changing from network to parallel, and then σ_x reduces to below σ_f with the crack distribution changing from parallel to no crack.

The insulation preheating laser cladding

The preheating laser cladding (pre-LC) can obtaine crack-free Ni60A coating when the preheating temperature is up to 500 °C, which is much higher than the martensitic transformation temperature of 45 steel substrate. It can increase deformation of the substrate and thermal damage of the substrate performance. While, the lower the cooling rate is benefit to reducing residual stress in the coating due to the more

Figure 10 Network crack distribution of coating, **a** Workpiece picture, **b** Schematic diagram of crack and stress.
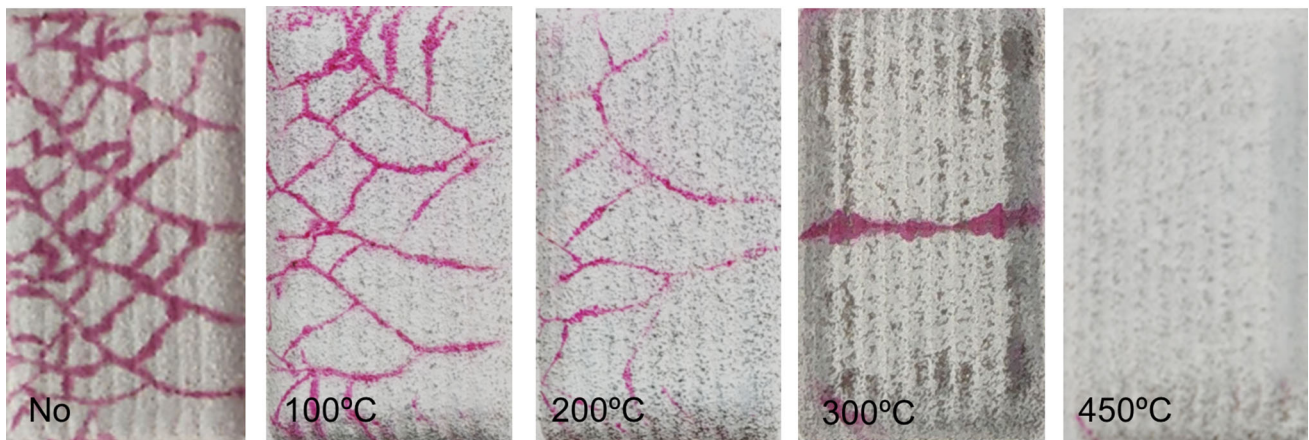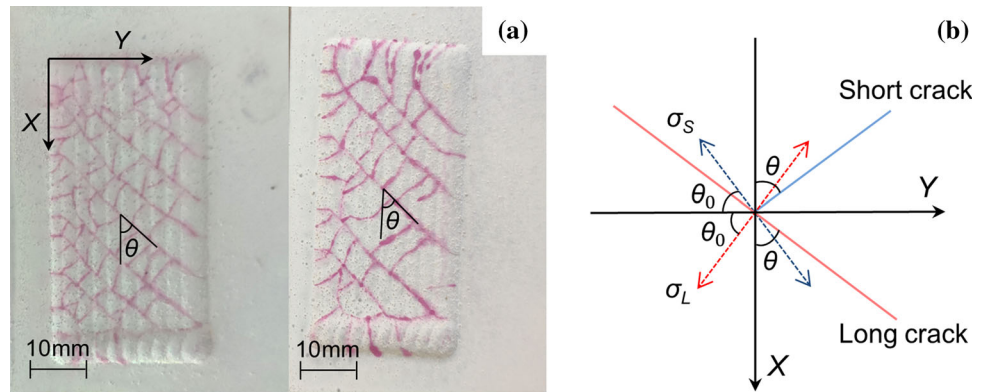

Figure 11 Influence of preheating temperature on crack distribution.

adequate plastic flow [26]. Thus, the lower the cooling rate combined with a lower preheating temperature also can prevent crack. In order to reduce the cooling rate further, an insulated plank is placed under the substrate, which can prevent thermal conduction between substrate and workbench and lead to lower dissipation efficiency. The insulated plank is asbestos board with the dimension of 200 mm × 200 mm × 20 mm. Using two-color pyrometer and thermocouple, respectively, the temperature measuring experiments of molten pool and substrate are designed to analyze the influence of the insulated plank.

The process parameters of cladding with or without insulated plank are $P = 1200$ W, $V_s = 6$ mm/s, $V_f = 0.179$ g/s. The measured temperature curve of molten pool and substrate is shown as Fig. 12. The results show that the insulated plank has almost no influence on the maximum temperature of molten pool, but it has an influence on the cooling rate of molten pool as shown in Fig. 12a and Table 3. After calculation, the cooling rate falls from 1292.7 °C/s to 1086.6 °C/s, and it helps to reduce the residual stress. The temperature of the substrate surface with insulated plank is always higher than that without insulated plank, as shown in Fig. 12b. And, the temperature differences between them increase with the increasing track number. When the cladding process is completed, the temperature difference is up to 67 °C, which reduces the temperature gradient between substrate and coating. As a result, the insulated plank is helpful to reduce cracking susceptibility of Ni60A coating in laser cladding, however, it cannot prevent crack completely for most of process parameters.

Therefore, the advantages of preheating and adding insulated plank are combined in laser cladding, that is the insulation preheating laser cladding (insulation pre-LC), to prevent crack at lower preheating temperature. The influence of pre-LC and insulation pre-LC on cracking rate is compared as shown in Fig. 13, and the relevant experiment parameters are listed in Table 4. The results show that the cracking rate of insulation pre-LC is much smaller than that of
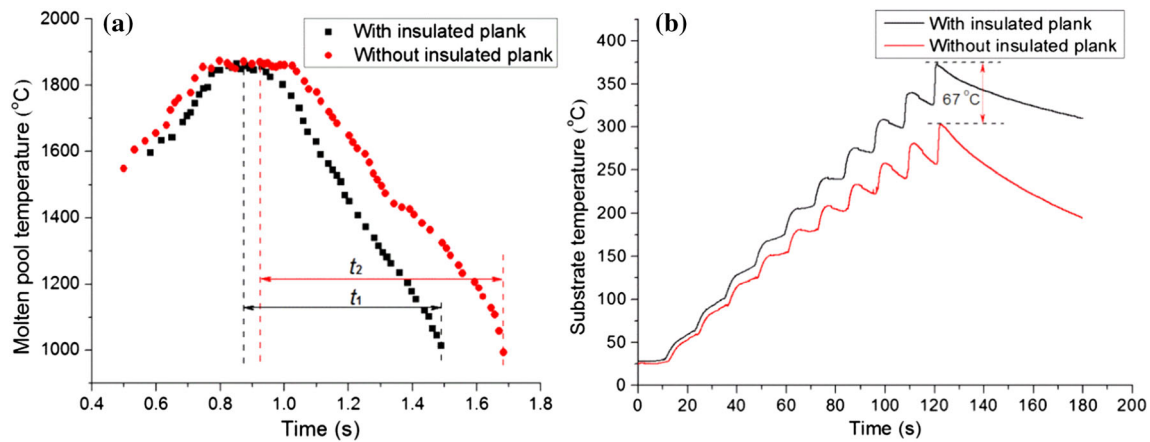
Figure 12 Temperature curve of **a** molten pool, **b** substrate.

Table 3 Temperature measurement result of molten pool

T_{max} (°C)	Time interval Δt (s)	Average cooling rate (°C/s)	Insulated plank
1850.2	0.658	1292.7	Without
1854.5	0.782	1086.6	With
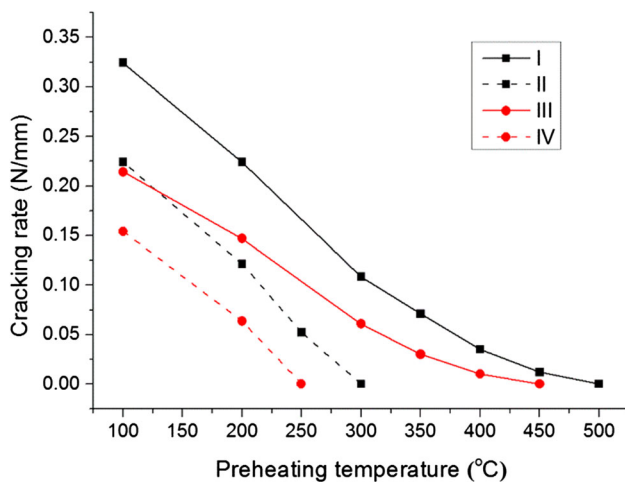
Figure 13 Influence of three preheating process on cracking rate.

Figure 14 Distribution of residual stress in coating.

Table 4 Experiment parameters of pre-LC and insulation pre-LC

No	Laser power (W)	Scanning speed (mm/s)	Powder feed rate (g/s)	Insulated plank
I	800	5	0.179	Without
II	800	5	0.179	With
III	1200	7	0.133	Without
IV	1200	7	0.133	With

pre-LC at the same preheating temperature. The crack can be prevented when preheated to 300 °C with insulated plank, which is lower than the required preheating temperature without insulated plank. Therefore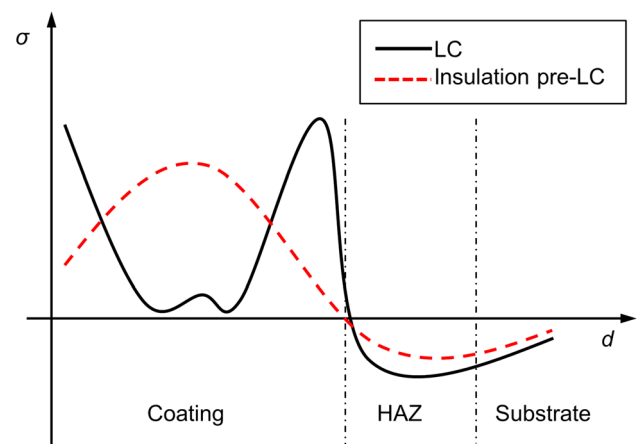, the insulation pre-LC is a better cladding method than pre-LC, which can obtain crack-free Ni60A coating with a larger range of process parameter and less damage of the substrate.

The insulation pre-LC can not only reduce residual stress but also changes stress distribution in coating.

As shown in Fig. 14, two stress peaks are located near the top and bottom of coating prepared by LC, while only one stress peak is located near the middle of coating prepared by insulation pre-LC [8]. Due to the lower dissipation efficiency of insulation pre-LC, the solidification sequence of molten pool changes significantly. Firstly, the top and bottom in molten pool are solidified, and then the middle of molten pool is solidified. As a result, the maximum tensile stress occurs at the middle of the coating. In addition, the lower cooling rate of substrate can reduce or even eliminate the Martensite transformation in HAZ, so the phase transformation stress at the bottom of the coating is little [26]. Therefore, there is only one stress peak located near the middle of coating, and this distribution of residual stress helps to prevent crack of Ni60A coating.

Figure 15 shows cross-sectional OM morphologies of the Ni60A coating prepared by LC, pre-LC with preheating 500 °C, insulation pre-LC with preheating 300 °C, respectively. It can be seen that the microstructure of the coatings is typical rapid solidification structure [30]. These three coatings have similar microstructure distribution of coatings. A bonding line (zone) at the coating/substrate interface indicates that the coating is metallurgically bonded with the substrate. The planar growth and cellular are found at this interface. As the distance to the interface increases, the columnar dendrite and equiaxed crystal are observed in the middle and top of the coating, respectively [31]. While, the grain size of the three coatings is different, especially the middle and top of the coatings. The coating (a) has the smallest grain size, while the coating (b) has the largest grain size. And the microhardness increases with
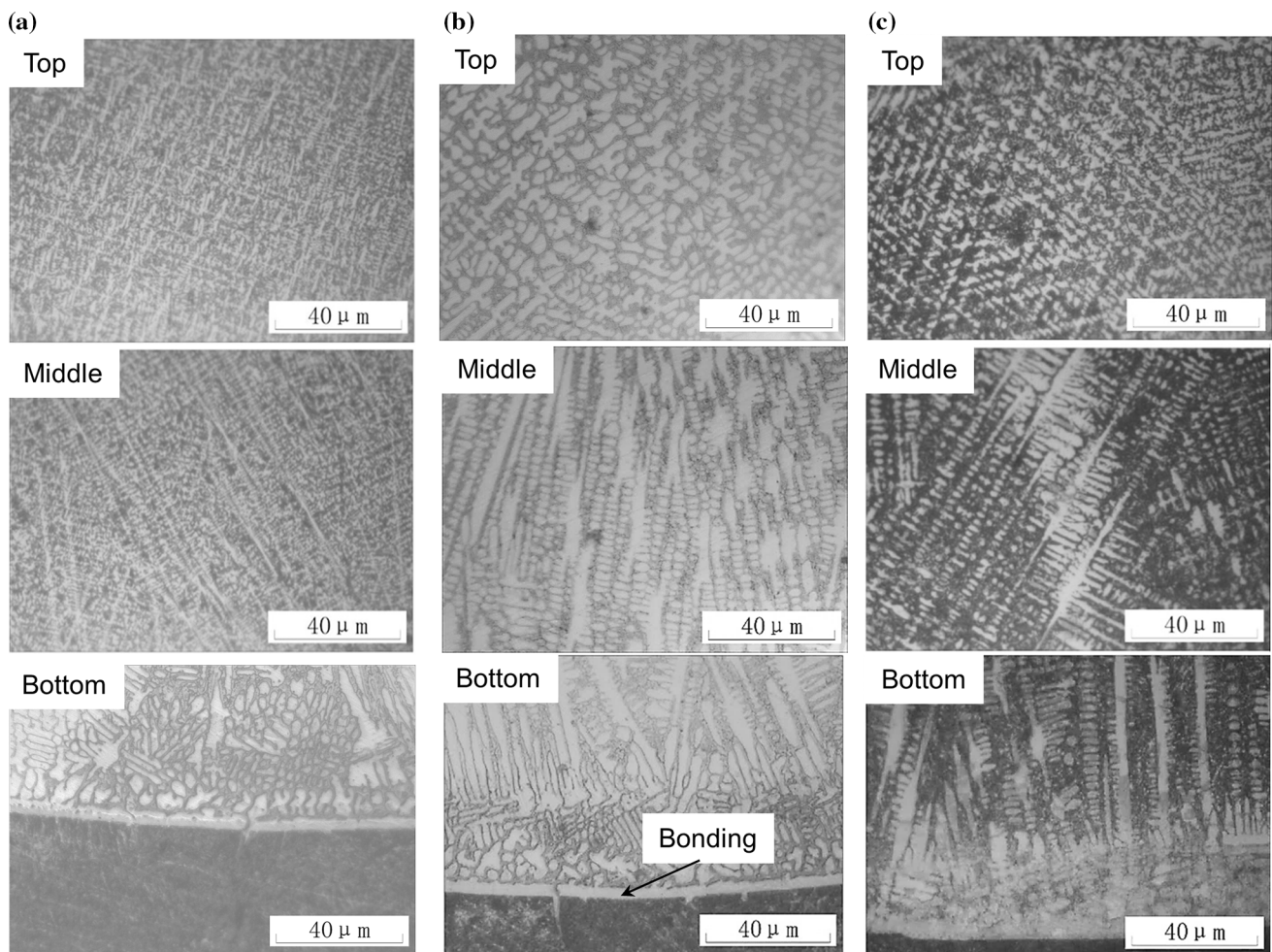

Figure 15 Cross-sectional OM morphologies of Ni60A coating, **a** LC, **b** Pre-LC with preheating 500 °C, **c** Insulation pre-LC with preheating 300 °C.

the decreasing grain size. Therefore, the microhardness of the coating prepared by LC is maximum, and the microhardness of the coating prepared by pre-LC with preheating 500 °C is minimum. The microhardness of the coating prepared by insulation pre-LC with preheating 300 °C is in between. This result is basically consistent with the microhardness difference of three coatings as shown in Fig. 16.

Due to large amount and nonuniformly distributed hard Cr-rich precipitates, the coating prepared by LC has high microhardness (642–705 HV) and large fluctuation of microhardness, but it has obvious cracks. Conversely, the coatings prepared by pre-LC with preheating 500 °C and insulation pre-LC with preheating 300 °C are not cracking, and the microhardness of two coatings decline and the fluctuation of microhardness are small. It is mainly due not only to the adequate plastic flow caused by lower cooling rate but also to the improved toughness caused by higher dilution rate of coating. Among two crack-free coatings, the latter has relatively higher microhardness (510–553 HV) which is about 2.7 times that of 45 steel substrate (approximately 200 HV). It is attributed to the presence of a certain amount of hard phase such as Cr-rich precipitates and eutectic structures in the coating. Therefore, the insulation pre-LC can obtain crack-free Ni60A coating with higher microhardness and less thermal damage of the substrate compared with the pre-LC.
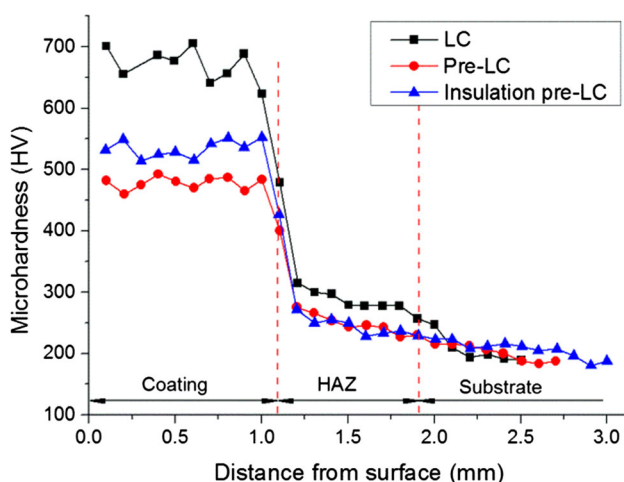

Figure 16 Microhardness profile of coating cladded by three process methods.

Conclusions

In this study, the Ni60A coating is prepared on 45 steel substrate by coaxial laser cladding, and the crack behavior and prevention method are studied. The conclusions are as follows:

(1) The nonuniform hard precipitates CrB, Cr_7C_3, $Cr_{23}C_6$ or incomplete melting powder is the main reason for high cracking susceptibility of Ni60A coating. By laser cladding, the cracking rate of coating decreases with the increasing line energy and the decreasing powder feed rate. The crack-free Ni60A coating can be obtained when the line energy is up to 800 J/mm in the condition $V_f = 0.133$ g/s. Also it can be obtained when the powder feed rate is down to 0.087 g/s in the condition $P = 1600$ W and $V_s = 3$ mm/s.

(2) According to the great difference of thermo-physical properties and temperature between the coating and the substrate, the thermal stress models are established. Among them, σ_z is much smaller than σ_y and σ_x, and σ_y is smaller than σ_x. Due to the change in the relative relationship among σ_x, σ_y and σ_f, the crack distribution changes from network to parallel, until to no crack with the increasing line energy and the decreasing powder feed rate. Also, the crack distribution has same change with the increasing preheating temperature. The angle between the direction of resultant stress of σ_x and σ_y and Y-axis $\theta_0 = \arctan(\sigma_x/\sigma_y) = 52.85° \in (50°, 54°)$, which fits with the direction of long and short cracks in network crack distribution.

(3) The substrate preheating has a great influence on cracking rate, and the crack can be prevented when preheated up to 500 °C. In order to reduce thermal damage of high preheating temperature to the substrate, the insulation pre-LC is studied to reduce cooling rate further to decrease cracking susceptibility. Using this method, the crack can be prevented when preheated to 300 °C, and the obtained Ni60A coating has finer microstructure and higher microhardness which is about 2.7 times as much as that of 45 steel substrate.

Acknowledgements

Declarations

Conflict of interest   The authors declare that there is no conflict of interests regarding the publication of this article.

References

[1] Sexton L, Lavin S, Byrne G, Kennedy A (2002) Laser cladding of aerospace materials. J Mater Process Technol 122(1):63–68. https://doi.org/10.1016/S0924-0136(01)01121-9

[2] Paul CP, Jain A, Ganesh P, Negi J, Nath AK (2006) Laser rapid manufacturing of Colmonoy-6 components. Opt Laser Eng 44(10):1096–1109. https://doi.org/10.1016/j.optlaseng.2005.08.005

[3] Weng F, Chen CZ, Yu HJ (2014) Research status of laser cladding on titanium and its alloys: a review. Mater Des 58:412–425. https://doi.org/10.1016/j.matdes.2014.01.077

[4] Fu FX, Zhang YL, Chang GG, Dai J (2016) Analysis on the physical mechanism of laser cladding crack and its influence factors. Optik 127(1):200–202. https://doi.org/10.1016/j.ijleo.2015.10.043

[5] De Oliveira U, Ocelík V, De Hosson JTM (2005) Analysis of coaxial laser cladding processing conditions. Surf Coat Technol 197(2–3):127–136. https://doi.org/10.1016/j.surfcoat.2004.06.029

[6] Zhou SF, Zeng XY, Hu QW, Huang YJ (2008) Analysis of crack behavior for Ni-based WC composite coatings by laser cladding and crack-free realization. Appl Surf Sci 255(5):1646–1653. https://doi.org/10.1016/j.apsusc.2008.04.003

[7] Wang DS, Liang EJ, Chao MJ, Yuan B (2008) Investigation on the microstructure and cracking susceptibility of laser-clad V_2O_5/NiCrBSiC alloy coatings. Surf Coat Technol 202(8):1371–1378. https://doi.org/10.1016/j.surfcoat.2007.06.036

[8] Huang YJ, Zeng XY (2010) Investigation on cracking behavior of Ni-based coating by laser-induction hybrid cladding. Appl Surf Sci 256(20):5985–5992. https://doi.org/10.1016/j.apsusc.2010.03.106

[9] Hemmati I, Ocelík V, De Hosson JTM (2012) Dilution effects in laser cladding of Ni–Cr–B–Si–C hardfacing alloys. Mater Lett 84:69–72. https://doi.org/10.1016/j.matlet.2012.06.054

[10] Chen ZH, Li RF, Gu JY, Zhang ZY, Tao YW, Tian YT (2020) Laser cladding of Ni60+17-4PH composite for a cracking-free and corrision resistive coating. Int J Mod Phys B 34(1–3):2040042. https://doi.org/10.1142/S0217979220400421

[11] Zhang P, Ma L, Yuan JP, Yin XN, Cai ZH (2008) The finite element simulation research on stress-strain field of laser cladding. Key Eng Mater 373–374:322–325

[12] Brückner F, Lepski D, Beyer E (2007) Modeling the influence of process parameters and additional heat sources on residual stresses in laser cladding. J Therm Spray Technol 16(3):355–373. https://doi.org/10.1007/s11666-007-9026-7

[13] Hemmati I, Ocelík V, De Hosson JTM (2013) Effects of the alloy composition on phase constitution and properties of laser deposited Ni–Cr–B–Si coatings. Phys Proc 41:302–311. https://doi.org/10.1016/j.phpro.2013.03.082

[14] Xu GJ, Kutsuna M, Liu ZJ, Zhang H (2006) Characteristics of Ni-based coating layer formed by laser and plasma cladding processes. Mater Sci Eng A 417(1–2):63–72. https://doi.org/10.1016/j.msea.2005.08.192

[15] Wang HY, Zuo DW, Sun YL, Xu F, Zhang D (2009) Microstructure of nanometer Al_2O_3 dispersion strengthened Ni-based high-temperature protective coatings by laser cladding. Trans Nonferrous Met Soc China 19(3):586–591. https://doi.org/10.1016/S1003-6326(08)60317-9

[16] Guo C, Chen JM, Zhou JS, Zhao JR, Wang LQ, Yu YJ, Zhou HD (2012) Effects of WC-Ni content on microstructure and wear resistance of laser cladding Ni-based alloys coating. Surf Coat Technol 206(8–9):2064–2071. https://doi.org/10.1016/j.surfcoat.2011.06.005

[17] Wang CL, Gao Y, Wang R, Wei DQ, Cai M, Fu YK (2018) Microstructure of laser-clad Ni60 cladding layers added with different amounts of rare-earth oxides on 6063 Al alloys. J Alloy Compd 740:1099–1107. https://doi.org/10.1016/j.jallcom.2018.01.061

[18] Zhai LL, Wang Q, Zhang JW, Ban CY (2019) Effect of alternating current electric field on microstructure and properties of laser cladding Ni–Cr–B–Si coating. Ceram Int 45(14):16873–16879. https://doi.org/10.1016/j.ceramint.2019.05.230

[19] Ning FD, Cong WL (2020) Ultrasonic vibration-assisted (UV-A) manufacturing processes: state of the art and future perspectives. J Manuf Process 51:174–190. https://doi.org/10.1016/j.jmapro.2020.01.028

[20] Wang FJ, Mao HD, Zhang DW, Zhao XY, Shen Y (2008) Online study of cracks during laser cladding process based

on acoustic emission technique and finite element analysis. Appl Surf Sci 255(5):3267–3275. https://doi.org/10.1016/j.apsusc.2008.09.039

[21] Jendrzejewski R, Śliwiński G, Krawczuk M, Ostachowicz W (2004) Temperature and stress fields induced during laser cladding. Comput Struct 82(7–8):653–658. https://doi.org/10.1016/j.compstruc.2003.11.005

[22] Jendrzejewski R, Śliwiński G, Krawczuk M, Ostachowicz W (2006) Temperature and stress during laser cladding of double-layer coatings. Surf Coat Technol 201(6):3328–3334. https://doi.org/10.1016/j.surfcoat.2006.07.065

[23] Zhou SF, Huang YJ, Zeng XY (2008) A study of Ni-based WC composite coatings by laser induction hybrid rapid cladding with elliptical spot. Appl Surf Sci 254(10):3110–3119. https://doi.org/10.1016/j.apsusc.2007.10.062

[24] Irwin GR (1962) Crack-extension force for a part-through crack in a plate. J Appl Mech 29(4):651–654. https://doi.org/10.1115/1.3640649

[25] Hemmati I, Ocelík V, Csach K, de Hosson JTM (2014) Microstructure and phase formation in a rapidly solidified laser-deposited Ni–Cr–B–Si–C hardfacing alloy. Metall Mater Trans A 45(2):878–892. https://doi.org/10.1007/s11661-013-2004-4

[26] Wang DZ, Hu QW, Zeng XY (2015) Residual stress and cracking behaviors of $Cr_{13}Ni_5Si_2$ based composite coatings prepared by laser-induction hybrid cladding. Surf Coat Technol 274:51–59. https://doi.org/10.1016/j.surfcoat.2015.04.035

[27] Liyanage T, Fisher G, Gerlich AP (2010) Influence of alloy chemistry on microstructure and properties in NiCrBSi overlay coatings deposited by plasma transferred arc welding (PTAW). Surf Coat Technol 205(3):759–765. https://doi.org/10.1016/j.surfcoat.2010.07.095

[28] Martinez Hurtado A, Francis JA, Stevens NPC (2016) An assessment of residual stress mitigation strategies for laser clad deposits. Mater Sci Technol 32(14):1484–1494. https://doi.org/10.1080/02670836.2016.1192766

[29] Albert Sue J, Schajer GS (1998) Stress determination for coatings. In: Lampman SR, Reidenbach F (eds) Surface engineering. ASM handbook. ASM International Materials Park (OH), Almere

[30] Zhou SF, Zeng XY (2010) Growth characteristics and mechanism of carbides precipitated in WC–Fe composite coatings by laser induction hybrid rapid cladding. J Alloys Compd 505(2):685–691. https://doi.org/10.1016/j.jallcom.2010.06.115

[31] Zhang J, Hu Y, Tan XJ, Guo L, Zhang QM (2015) Microstructure and high temperature tribological behavior of laser cladding Ni60A alloys coatings on 45 steel substrate. Trans Nonferrous Met Soc China 255(5):1525–1532. https://doi.org/10.1016/S1003-6326(15)63754-2